KAPITEL 3 / *CHAPTER 3* [17]
EFFICIENCY OF MACHINE LEARNING OF PSYCHOPHYSIOLOGICAL STATE CLASSIFIERS BASED ON EYE TRACKING DATA IN ORTHOGONAL DIRECTIONS

DOI: 10.30890/2709-2313.2025-42-04-027

Introduction

The level of development of science and technology in the XXI century has significantly expanded the possibilities for analyzing human behavior and cognitive activity, with eye-tracking technologies becoming an essential research instrument. The human eye movement system (EMS) provides highly informative parameters that reflect neurological function, psychophysiological states, and cognitive load, making it a valuable object of investigation across neuroscience, medicine, and artificial intelligence.

A substantial body of research has confirmed the clinical relevance of eye-tracking in diagnosing and monitoring neurological impairments. For instance, ocular parameters have been systematically examined in Parkinson's disease, supporting retrospective clinical assessment [1], while anomaly detection techniques have been applied to parametric and nonparametric analyses of EMS data [2]. Eye-tracking biomarkers have also been proposed to improve the diagnostic accuracy of autism in primary care [3], and the study of oculomotor features has contributed to the development of intervention systems for dyslexia [4]. Beyond clinical diagnosis, eye movement parameters are widely used to assess eye fatigue [5] and to measure cognitive load during human-computer interaction tasks under time-critical conditions [6]. Furthermore, predictive models based on eye-tracking have demonstrated potential in estimating higher-level cognitive functions, such as reading comprehension [7] and expert-novice differences during surgical training [8].

Recent advances in artificial intelligence have further enhanced the applicability of EMS data for medical diagnostics. Deep learning approaches have been proposed

[17]***Authors:*** *Pavlenko Vitaliy D., Lukashuk Denys K.*
Number of characters: *35785*
Author's sheets: *0,90*

for Alzheimer's disease detection using eye-tracking data [9], while transfer learning techniques have improved generalization in eye disease recognition systems [10]. At the same time, nonlinear system identification provides a methodological framework for modeling EMS dynamics. Integral models in the form of Volterra polynomials have been applied for the identification of neurophysiological signals [11], and Volterra-Laguerre models have been successfully employed to describe smooth pursuit eye movements [12]. These methods are supported by established theoretical foundations of Volterra-based system identification [13].

In addition to their biomedical relevance, eye-tracking technologies are increasingly utilized in diverse applied domains. They have been adopted to evaluate teamwork performance in healthcare [14], to enable secure biometric authentication based on spatiotemporal gaze patterns [15], and to support nonlinear analyses of motor imagery [16]. In education, eye-tracking has been used to study cognitive processes in children during mental calculation [17] and to characterize learners' attentional states in multimedia learning environments [18]. Moreover, EMS data are applied in brain-computer interface research, including EEG artifact reduction [19], in software engineering tasks to identify source code defects [20], and in professional training for vision-intensive domains such as aviation [21].

Therefore, eye-tracking research represents a rapidly evolving interdisciplinary field, combining medical, cognitive, and engineering perspectives. In this study, we focus on modeling EMS dynamics using nonlinear Volterra models, aiming to improve the accuracy of system identification and to provide methodological support for psychophysiological state assessment and applied developments across healthcare, education, and artificial intelligence.

3.1 Problem Statement

The human EMS reflects essential cognitive and psychophysiological processes, and its modeling provides valuable tools for assessing the functional state of the central nervous system. Conventional approaches to eye movement analysis mainly rely on empirical methods and simplified parametric models, which often fail to capture the

nonlinear dynamic properties of the EMS. In contrast, integral nonlinear models, in particular first- and second-order Volterra representations in the form of transient characteristics, have demonstrated significant potential for improving the diagnostic evaluation of psychophysiological states [22].

The objective of the present study is to examine the diagnostic effectiveness second-order Volterra models of the EMS, obtained from experimental "input-output" eye-tracking data. Unlike previous studies, where test stimuli were applied exclusively in the horizontal direction, the current work expands the experimental design by including both horizontal and vertical trajectories of visual stimulation. This extension enables a more comprehensive assessment of the EMS and allows for analyzing the effect of stimulus direction on the accuracy of psychophysiological state classification.

The subject of investigation comprises computational methods and software tools for extracting diagnostic features from EMS identification data, parameterized as first- and second-order transient characteristics. Particular attention is given to the formation of feature spaces and the construction of classifiers, including Bayesian and Support Vector Machine approaches, with a focus on evaluating how the choice of stimulus direction influences the classification performance.

This research represents a further step in the development of intelligent information technologies for psychophysiological state assessment, advancing earlier approaches by introducing multidirectional EMS identification and systematically studying its impact on diagnostic reliability.

3.2 Theoretical Background

For the identification of the nonlinear dynamic system (NDS), mathematical models in the form of Volterra integro-power polynomials are employed. The least squares method (LSM) [23] is used for EMS identification. In this study, two models are utilized for EMS identification: Model1 and Model2. Model1 is based on horizontal test visual stimuli, whereas Model2 is constructed from orthogonal vertical test experiments.

The time-domain identification method is applied for building Model1, which is

based on approximating the response $y(t)$ of the NDS to a input deterministic signal $x(t)$ by an integro-power polynomial of order N (where N is the order of the approximation model):

$$y_N(t) = \sum_{n=1}^{N} \hat{y}_n(t) = \sum_{n=1}^{N} \int_0^t \dots \int_0^t w_n(t-\tau_1,\dots,t-\tau_n) \prod_{i=1}^{n} x(\tau_i) d\tau_i, \quad (1)$$

where $\hat{y}_n(t)$ denotes the partial components of the model response (with n being the convolution dimension), and $w_n(t-\tau_1,\dots, t-\tau_n)$ – is the Volterra kernel of order n.

The following statement holds [23].

Statement. Let the test signals $a_1x(t)$, $a_2x(t)$, …, $a_Lx(t)$ be sequentially applied to the input of the NDS; $L \geq N$; a_1, a_2,…,a_L – are distinct real numbers satisfying the condition $0< a_j \leq 1$, for $\forall j=1,2,...,L$; and $x(t)$ is an deterministic signal. Then:

$$\tilde{y}_N(a_j x(t)) = \sum_{n=1}^{N} \hat{y}_n(a_j x(t)) =$$
$$= \sum_{n=1}^{N} a_j^n \int_0^t \dots \int_0^t w_n(t-\tau_1,\dots,t-\tau_n) \prod_{i=1}^{n} x(\tau_i) d\tau_i = \sum_{n=1}^{N} a_j^n \hat{y}_n(t). \quad (2)$$

The partial components $\hat{y}_n(t)$ in the approximation model are determined using the LSM. This makes it possible to obtain such estimates, for which the sum of squared deviations of the responses of the identified NDS $y(a_j x(t)) = y(t \mid a_j)$ from the responses of the model $\tilde{y}_N(a_j x(t))$ is minimized, i.e., it ensures the minimum of the mean square error criterion. The minimization of the criterion reduces to solving the system of Gauss normal equations, which can be written in vector-matrix form as:

$$\mathrm{A}'\mathrm{A}\hat{\mathrm{y}} = \mathrm{A}'\mathrm{y}, \quad (3)$$

where

$$\mathrm{A} = \begin{bmatrix} a_1 & a_1^2 & \cdots & a_1^N \\ a_2 & a_2^2 & \cdots & a_2^N \\ \cdots & \cdots & \cdots & \cdots \\ a_L & a_L^2 & \cdots & a_L^N \end{bmatrix}, \quad \mathrm{y} = \begin{bmatrix} y(t \mid a_1) \\ y(t \mid a_2) \\ \cdots \\ y(t \mid a_L) \end{bmatrix}, \quad \hat{\mathrm{y}} = \begin{bmatrix} \hat{y}_1(t) \\ \hat{y}_2(t) \\ \cdots \\ \hat{y}_N(t) \end{bmatrix},$$

and A' denotes the transposed matrix.

From equation (3), we obtain

$$\hat{\mathrm{y}} = (\mathrm{A}'\mathrm{A})^{-1}\mathrm{A}'\mathrm{y}\,, \tag{4}$$

If step test signals with amplitudes a_1, a_2,…,a_L, are applied to the input of the system to be identified, the estimates of the transient characteristics $\hat{h}_1^{(N)}(t) = \hat{y}_1(t)$ and diagonal cross-sections of the NDS transient characteristics $\hat{h}_2^{(N)}(t,t) = \hat{y}_2(t)$, …, $\hat{h}_N^{(N)}(t,...,t) = \hat{y}_N(t)$ are obtained [23].

The responses of the investigated EMS models in the general case are computed on the basis of the expression:

$$\tilde{y}_j(t \mid a_j) = a_j\hat{y}_1(t) + a_j^2\hat{y}_2(t) + ... + a_j^N\hat{y}_N(t), \tag{5}$$

Model2, based on vertical orthogonal data, is constructed analogously to Model1. The test signals $b_1u(t)$, $b_2u(t)$, …, $b_Lu(t)$ are applied sequentially to the input of the NDS, where b_1, b_2,…,b_L ($L \geq N$) are distinct real numbers satisfying the condition $0< b_j \leq 1$, for $\forall j$=1,2,...,L; and $u(t)$ is an input deterministic signal.

The partial components $\hat{z}_n(t)$ in the approximation model are determined using the LSM, ensuring that the sum of squared deviations of the responses of the identified NDS $z(b_j u(t)) = z(t \mid b_j)$ from the responses of the model $\tilde{z}_N(b_j u(t))$ is minimized. The minimization of the criterion reduces to solving the system of Gauss normal equations, which can be written in vector-matrix form as:

$$\mathrm{B}'\mathrm{B}\hat{z} = \mathrm{B}'z\,, \tag{6}$$

where

$$\mathrm{B} = \begin{bmatrix} b_1 & b_1^2 & \cdots & b_1^N \\ b_2 & b_2^2 & \cdots & b_2^N \\ \cdots & \cdots & \cdots & \cdots \\ b_L & b_L^2 & \cdots & b_L^N \end{bmatrix}, \quad \mathrm{z} = \begin{bmatrix} z(t \mid b_1) \\ z(t \mid b_2) \\ \cdots \\ z(t \mid b_L) \end{bmatrix}, \quad \hat{\mathrm{z}} = \begin{bmatrix} \hat{z}_1(t) \\ \hat{z}_2(t) \\ \cdots \\ \hat{z}_N(t) \end{bmatrix},$$

and B' denotes the transposed matrix.

From equation (6), we obtain

$$\hat{\mathrm{z}} = (\mathrm{B}'\mathrm{B})^{-1}\mathrm{B}'z\,, \tag{7}$$

If step test signals with amplitudes b_1, b_2,…,b_L, are applied to the input of the system to be identified, the estimates of the transient characteristics $\hat{g}_1^{(N)}(t) = \hat{z}_1(t)$ and diagonal cross-sections of the NDS transient characteristics $\hat{g}_2^{(N)}(t,t) = \hat{z}_2(t)$,…, $\hat{g}_N^{(N)}(t,...,t) = \hat{z}_N(t)$ are obtained in the same way as in Model1.

The responses of the EMS model, based on Model2, are computed using the expression:

$$\tilde{z}_j(t \mid b_j) = b_j \hat{z}_1(t) + b_j^2 \hat{z}_2(t) + ... + b_j^N \hat{z}_N(t), \quad (8)$$

3.3 EMS Data Acquisition Procedure

The problem of accuracy evaluation of EMS models based on Volterra series was previously investigated in [22], where three model orders and identification methods were compared. In the present study, the analysis is focused on the quadratic Volterra model identified by the LSM using step test signals of different amplitudes. The EMS response to test step signals of the form $x(t)=a_j\theta(t)$, j=1, 2, 3, where $\theta(t)$ denotes the Heaviside function, is analyzed with amplitudes a_j (j=1, 2, 3): $a_1=(1/3)l_x$, $a_2=(2/3)l_x$, $a_3=l_x$ (l_x denotes the screen width of a computer monitor in pixels) was investigated in the context of constructing Volterra models.

For vertical experiments, analogous EMS responses to test step signals are defined as $u(t)=b_k\theta(t)$ with amplitudes b_k (k=1, 2, 3): $b_1=(1/3)l_y$, $b_2=(2/3)l_y$, $b_3=l_y$ where l_y denotes the screen height in pixels.

For clarity, models derived from horizontal data are denoted as Model1, and those from vertical data as Model2.

For EMS identification, empirical data were obtained in "input-output" experiments using advanced eye-tracking technology. The Tobii Pro TX300 eye tracker was employed to record ocular responses to orthogonal step visual stimuli, presented separately along horizontal and vertical axes. Measurements were carried out at different times of the day, including "Morning" (before work) and "Evening" (after work), as well as on different days [24]. Each complete EMS research cycle for a single participant included three experiments with test signals of increasing amplitude,

performed sequentially along each axis.

During each EMS research cycle, the participant initially fixates on the starting position (red point). After a short delay (1-2 sec), the red point disappears, and a test stimulus (blue point) is presented (2-3 sec) at the first test amplitude along the corresponding axis. The red fixation point then reappears, allowing the participant to return gaze to the initial position. The same procedure is then repeated for the second and third test amplitudes, each separated by a brief interstimulus interval.

The horizontal experiment sequence is illustrated in Fig. 1, which show the initial fixation and successive presentations of the test stimulus at increasing horizontal positions. The corresponding raw eye-tracking signals for horizontal displacements are presented in Fig. 2 for the "Morning" and "Evening" conditions.

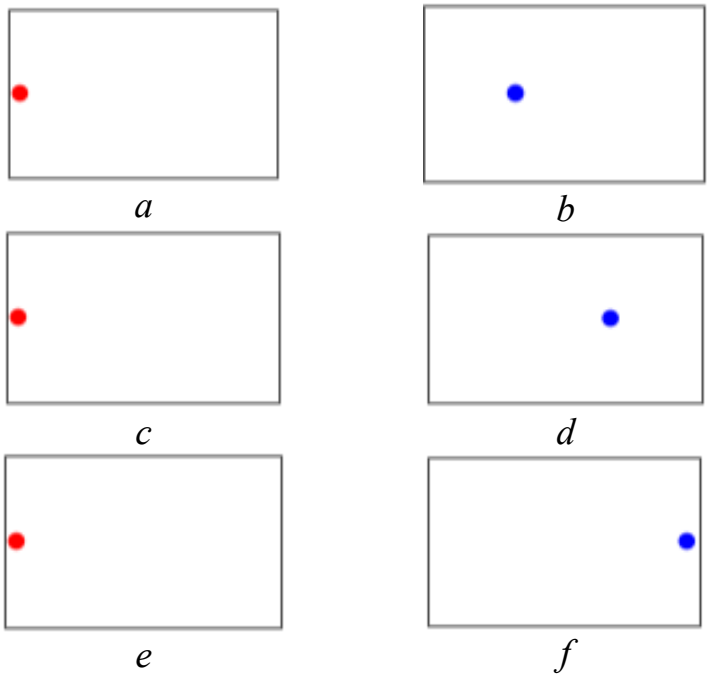

Figure 1 – Test stimulus: *a*), *c*), *e*) – initial position; *b*) – test stimulus position (a_1 = 1/3); *d*) – test stimulus position (a_2 = 2/3); *f*) – test stimulus position (a_3 = 1)

A source: Created by the authors.

The vertical experiment follows an analogous procedure, with stimuli presented from the top toward the bottom of the screen. The initial fixation and successive vertical positions of the test stimulus are illustrated in Fig. 3, and the corresponding raw eye-tracking signals are shown in Fig. 4 for the "Morning" and "Evening" conditions.

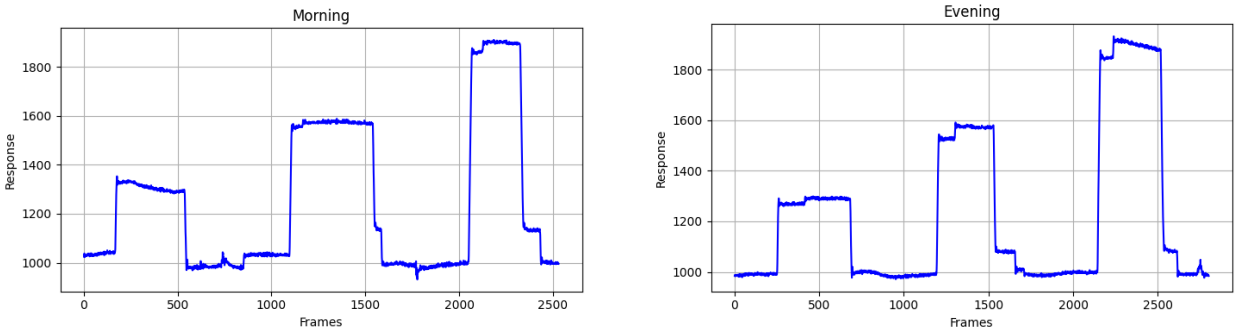

a *b*

Figure 2 – Raw eye tracker output signals recorded during horizontal experiments for the respondent's state: *a*) "Morning", *b*) "Evening"

A source: Created by the authors.

The vertical experiment follows an analogous procedure, with stimuli presented from the top toward the bottom of the screen. The initial fixation and successive vertical positions of the test stimulus are illustrated in Fig. 3, and the corresponding raw eye-tracking signals are shown in Fig. 4 for the "Morning" and "Evening" conditions.

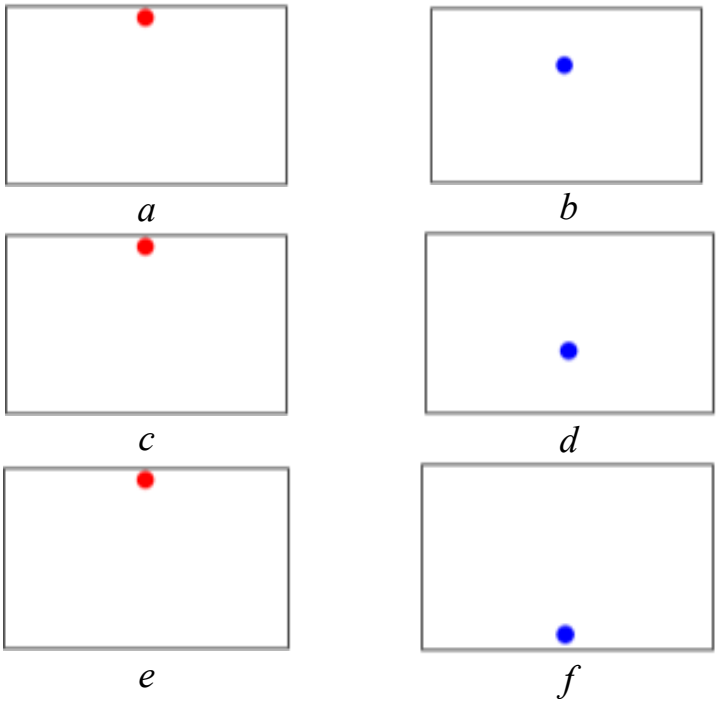

Figure 3 – Test stimulus: *a*), *c*), *e*) – initial position; *b*) – test stimulus position (b_1 = 1/3); *d*) – test stimulus position (b_2 = 2/3); *f*) – test stimulus position (b_3 = 1)

A source: Created by the authors.

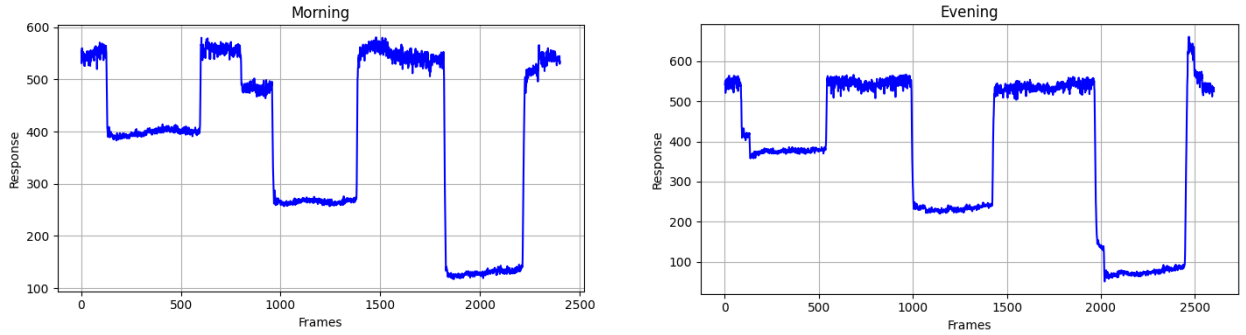

a *b*

Figure 4 – Raw eye tracker output signals recorded during vertical experiments for the respondent's state: *a*) "Morning", *b*) "Evening"

A source: Created by the authors.

3.4 EMS Model1 and Model2

This section investigates the specifics of applying empirical data to construct EMS models and evaluates the variability of averaged transient characteristics depending on the psychophysiological state of the subject in the "Morning" and "Evening" conditions. In accordance with the identification algorithm (3), all EMS response data were aligned to a common initial point (synchronization was performed).

The empirical data obtained from horizontal experiments are designated as Dataset1, while those from vertical experiments are designated as Dataset2. Dataset1 comprises eight observations corresponding to the "Morning" state and eight observations corresponding to the "Evening" state, as illustrated in Fig. 5. Dataset2 comprises seven observations for the "Morning" state and eight observations for the "Evening" state; to equalize the number of experiments, an additional eighth dataset was generated synthetically. The vertical experimental data are presented in Fig. 6.

EMS models Model1 and Model2 were constructed separately based on horizontal and vertical experimental data. The transient characteristics derived from the Dataset1 are denoted as $\hat{h}_1^{(N)}(t)$ and $\hat{h}_2^{(N)}(t,t)$ while those obtained from the Dataset2 are denoted as $\hat{g}_1^{(N)}(t)$ and $\hat{g}_2^{(N)}(t,t)$. The corresponding functions of the first and second order are presented in Fig. 7 and Fig. 8, respectively, together with their averaged values in the “Morning” and “Evening” states.

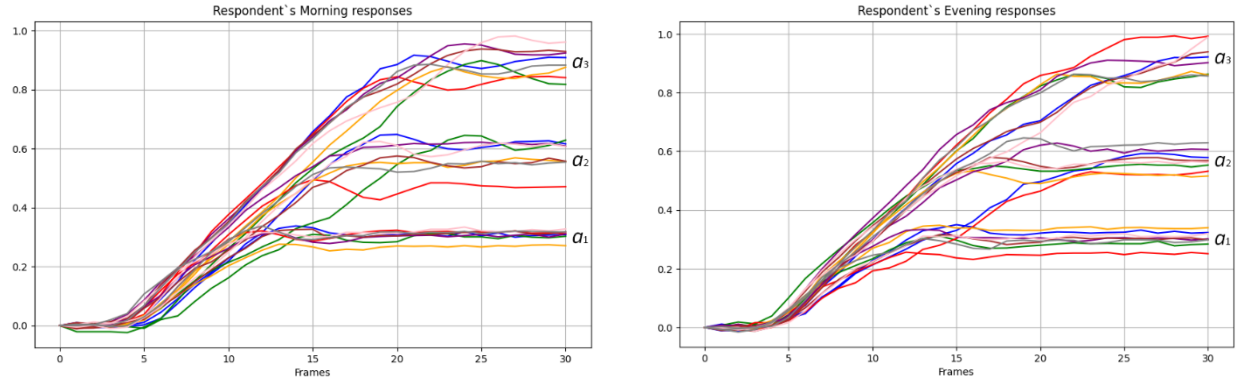

a *b*

Figure 5 – Dataset1 – Empirical eye movement responses in the horizontal direction for the states: *a*) "Morning"; *b*) "Evening"

A source: Created by the authors.

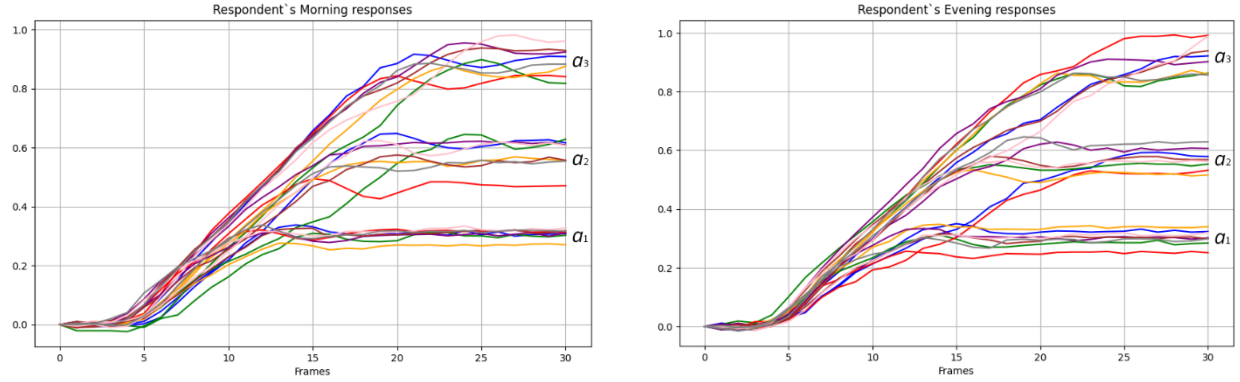

a *b*

Figure 6 – Dataset2 – Empirical eye movement responses in the vertical direction for the states: *a*) "Morning"; *b*) "Evening"

A source: Created by the authors.

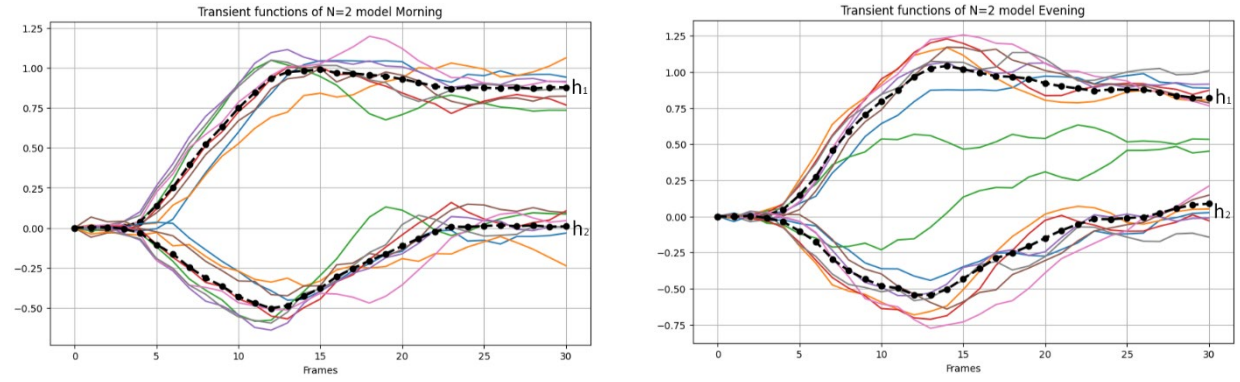

a *b*

Figure 7 – Transient characteristics of the first- and second-order of EMS Model1 obtained from Dataset1 and their averaged values in the states: *a*) "Morning"; *b*) "Evening"

A source: Created by the authors.

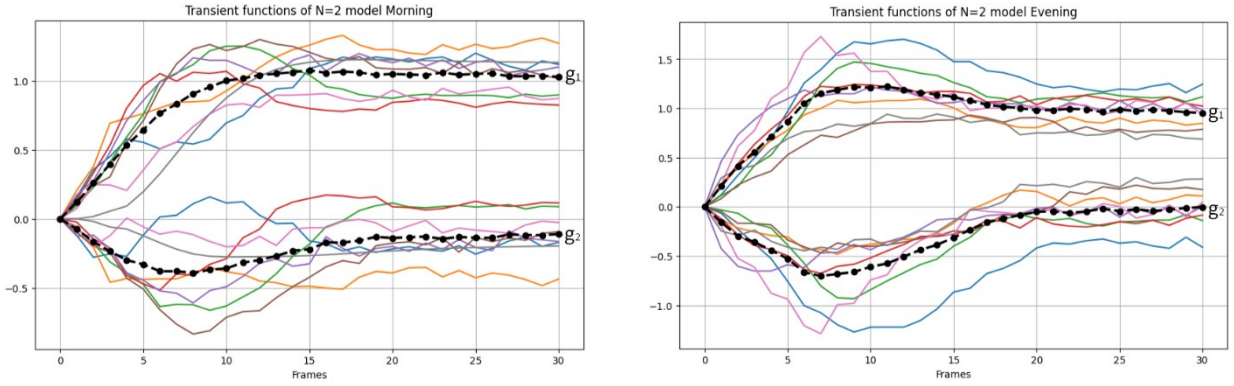

a *b*

Figure 8 – Transient characteristics of the first- and second-order of EMS Model2 obtained from Dataset2 and their averaged values in the states: *a*) "Morning"; *b*) "Evening"

A source: Created by the authors.

The variability (deviation) of the averaged transient characteristics of the EMS models Model1 for the respondent`s "Morning" $\hat{h}_{nN}^{(\mathrm{M})}(t_m)$ and "Evening" $\hat{h}_{nN}^{(\mathrm{E})}(t_m)$ conditions was evaluated using the following metrics:

σ_{nN} – maximum deviation

$$\sigma_{nN} = \max_{m\in[0,M]} |\hat{h}_{nN}^{(\mathrm{M})}(t_m) - \hat{h}_{nN}^{(\mathrm{E})}(t_m)|; \quad (9)$$

ε_{nN} – normalized root mean square deviation (NRMSD)

$$\varepsilon_{nN} = \left(\frac{\sum_{m=0}^{M} \left(\hat{h}_{nN}^{(\mathrm{M})}(t_m) - \hat{h}_{nN}^{(\mathrm{E})}(t_m) \right)^2}{\sum_{m=0}^{M} \left(\hat{h}_{nN}^{(\mathrm{M})}(t_m) \right)^2} \right)^{1/2}; \quad (10)$$

where $n = 1,2,\ldots,N$.

Using the transient characteristics of Model2, the metrics can be formally represented in the same form as formulas (9) and (10) by considering the "Morning" $\hat{g}_{nN}^{(\mathrm{M})}(t_m)$ and "Evening" $\hat{g}_{nN}^{(\mathrm{E})}(t_m)$ conditions.

The variability metrics of the averaged transient characteristics for Model1 and Model2 are presented in Table 1.

Table 1 – Variability indicators of the averaged transient characteristics for Model1 and Model2

Model	ε_{1N}	σ_{1N}	ε_{2N}	σ_{2N}
Model1	0.045	0.0706	0.2444	0.0796
Model2	0.1257	0.3209	0.7174	0.3226

A source: Calculated by the authors.

3.5. Dataset Formation

In this work, machine learning techniques are employed to evaluate the efficiency of feature spaces derived from linear and quadratic transient characteristics for the classification of psychophysiological states.

To facilitate further analysis, the following designations are used:

- E_0 – a feature space composed of heuristic parameters extracted from EMS Model1;
- $\tilde{E}_0$ – a feature space composed of heuristic parameters extracted from EMS Model2;
- W – a feature space obtained from approximation and detail coefficients produced by wavelet decomposition of the Model1 signal;
- $\tilde{W}$ – a feature space obtained from approximation and detail coefficients produced by wavelet decomposition of the Model2 signal;

3.5.1 Feature Space E_0 and $\tilde{E}_0$

The heuristic feature space E_0 is constructed using transient characteristics of the second-order Volterra model. The choice of these heuristic parameters is justified by earlier research, where they demonstrated both informativeness and sensitivity to variations in the subject's psychophysiological condition. The list of EMS heuristic features derived from the Model1 represents a subset of the features $e_k \in E_0, k = \overline{1,21}$ investigated in [25].

Table 2 – Heuristic features determined from first- and second-order transient characteristics of EMS Model1

Feature	Formal definition	Feature	Formal definition
e_1	$\sum_{m=0}^{M} \lvert \hat{h}_1(t_m) \rvert$	e_{11}	$\arg\min_{m\in[0,M]} \hat{h}_1'(t_m)$
e_2	$\sum_{m=0}^{M} \lvert \hat{h}_2(t_m, t_m) \rvert$	e_{12}	$\min_{m\in[0,M]} \hat{h}_2'(t_m, t_m)$
e_4	$\max_{m\in[0,M]} \hat{h}_1'(t_m)$	e_{13}	$\arg\min_{m\in[0,M]} \hat{h}_2'(t_m, t_m)$
e_5	$\arg\max_{m\in[0,M]} \hat{h}_1'(t_m)$	e_{16}	$\max_{m\in[0,M]} \lvert \hat{h}_1(t_m) \rvert$
e_6	$\max_{m\in[0,M]} \hat{h}_2'(t_m, t_m)$	e_{17}	$\arg\max_{m\in[0,M]} \lvert \hat{h}_1(t_m) \rvert$
e_7	$\arg\max_{m\in[0,M]} \hat{h}_2'(t_m, t_m)$	e_{18}	$\max_{m\in[0,M]} \lvert \hat{h}_2(t_m, t_m) \rvert$
e_{10}	$\min_{m\in[0,M]} \hat{h}_1'(t_m)$	e_{19}	$\arg\max_{m\in[0,M]} \lvert \hat{h}_2(t_m, t_m) \rvert$

A source: [25].

where $\hat{h}_1'(t_m)$ and $\hat{h}_2'(t_m, t_m)$ represent the derivatives of the first- and second-order transient characteristics, respectively.

The feature space $\tilde{\mathrm{E}}_0$ is formed analogously to E_0, following the definitions provided in Table 2, with the first- and second-order transient characteristics of Model2, $\hat{g}_1(t_m)$ and $\hat{g}_2(t_m, t_m)$, substituted for the corresponding Model1 characteristics. The list of EMS heuristic features derived from the Model2 represents a subset of the features $\tilde{e}_k \in \tilde{\mathrm{E}}_0, k = \overline{1,21}$.

3.5.2 Feature Space W and W̃

The W feature space is generated through wavelet decomposition [26] of the transient characteristics of the first and second order. The decomposition is performed using the discrete wavelet transform (DWT), where Coiflet 4 serves as the mother wavelet with a decomposition level of 2. The feature vector is formed from the first five approximation coefficients (*ca*) together with the first five detail coefficients (*cd*) obtained at the second decomposition level. Each feature in the W space is denoted as

$w_m \in \mathrm{W}, m = \overline{1,10}$, where $w_1 = ca[1]$, …, $w_5 = ca[5]$, $w_6 = cd[1]$,…, $w_{10} = cd[5]$; m is the feature index corresponding to the selected wavelet coefficients.

For Model1, the features of the feature space W are denoted as w_m, whereas for Model2, the corresponding features of the feature space $\tilde{\mathrm{W}}$ are denoted as $\tilde{w}_m$.

3.6 SVM Classifier

To assess the potential of the feature spaces in classifying psychophysiological states, a support vector machine (SVM) classifier with a Gaussian (RBF) kernel was implemented. The classifier was trained and evaluated in the Python environment using the sklearn.svm.SVC class from the Scikit-learn library. Classification performance metrics were calculated using functions from the sklearn.metrics module.

The efficiency of classification was evaluated based on the informativeness of different feature combinations using the probability of correct recognition (PCR) [25] criterion. An exhaustive search strategy was applied, which allowed for the consistent examination of all possible feature pairs in order to identify diagnostically valuable ones.

3.6.1 Dataset Based on Model1

Feature space E_0: For the EMS Model1, the maximum PCR reached 87.5% for the feature pair based on a combination of linear and quadratic transient characteristics:

$$\left(e_{10} = \min_{m\in[0,M]} \hat{h}_1^{'}(t_m) \right) \& \left(e_{12} = \min_{m\in[0,M]} \hat{h}_2^{'}(t_m, t_m) \right). \quad (11)$$

The corresponding confusion matrix illustrating the distribution of correctly and incorrectly classified samples is presented in Fig. 9.

Feature space W: For the W feature space, the highest PCR of 87.5% was obtained for the feature pairs $w_4\&w_8$ and $w_6\&w_8$.

3.6.2 Dataset Based on Model2

Feature space $\tilde{\mathrm{E}}_0$: For the EMS Model2, the maximum PCR was 87.5% for the

feature pairs based on a combination of linear and quadratic transient characteristics:

$$\left(\tilde{e}_2 = \sum_{m=0}^{M} |\hat{g}_2(t_m, t_m)|\right) \& \left(\tilde{e}_5 = \arg\max_{m\in[0,M]} \hat{g}_1^{'}(t_m)\right); \quad (12)$$

$$\left(\tilde{e}_7 = \arg\max_{m\in[0,M]} \hat{g}_2^{'}(t_m, t_m)\right) \& \left(\tilde{e}_{11} = \arg\min_{m\in[0,M]} \hat{g}_1^{'}(t_m)\right). \quad (13)$$

Feature space $\tilde{W}$: For the $\tilde{W}$ feature space, the highest PCR of 93.75% was obtained for the feature pair $\tilde{w}_7\&\tilde{w}_8$, and the corresponding confusion matrix is presented in Fig. 10.

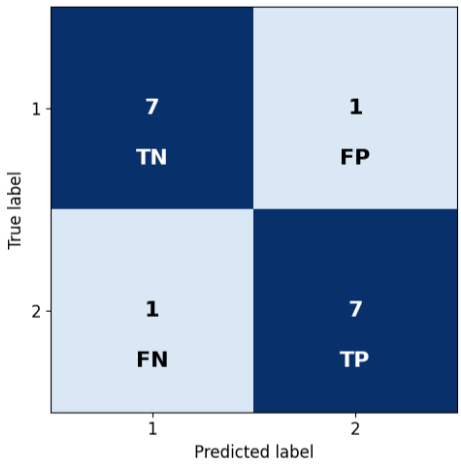

Figure 9 – Confusion Matrix for the classifier based on feature pair $e_{10}\&e_{12}$

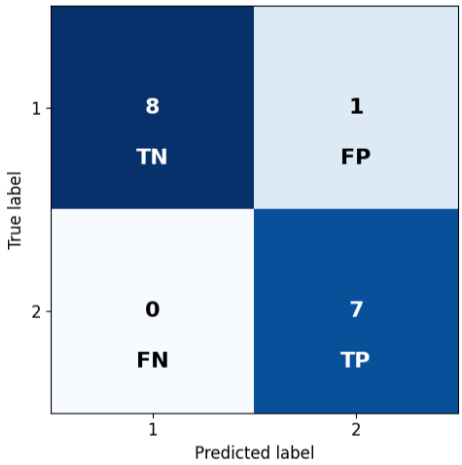

Figure 10 – Confusion Matrix for the classifier based on feature pair $\tilde{w}_7\&\tilde{w}_8$

A source: Calculated by the authors.

3.6.3 Dataset Based on Model1 and Model2

Feature space E_0 and $\tilde{E}_0$: For the combined Dataset1 and Dataset2, the EMS models achieved a maximum PCR of 93.75% for the feature pair Based on a combination of linear and quadratic transient characteristics:

$$\left(e_{12} = \min_{m\in[0,M]} \hat{h}_2^{'}(t_m, t_m)\right) \& \left(\tilde{e}_{10} = \min_{m\in[0,M]} \hat{g}_1^{'}(t_m)\right); \quad (14)$$

The classification performance associated with this feature pair is illustrated in the confusion matrix (Fig. 11) and the ROC curve (Fig. 12).

Additionally, several feature pairs with a PCR of 87.5% were identified, including:

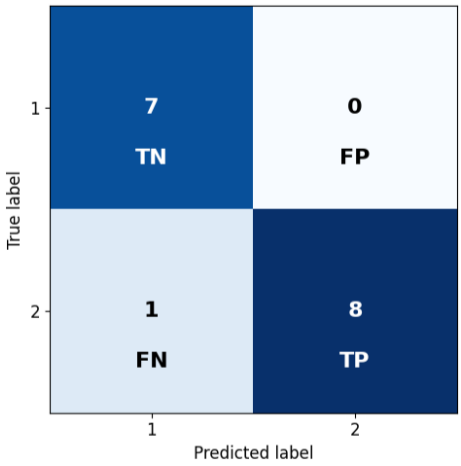

Figure 11 – Confusion Matrix for the classifier based on feature pair e_{12}&$\tilde{e}_{10}$

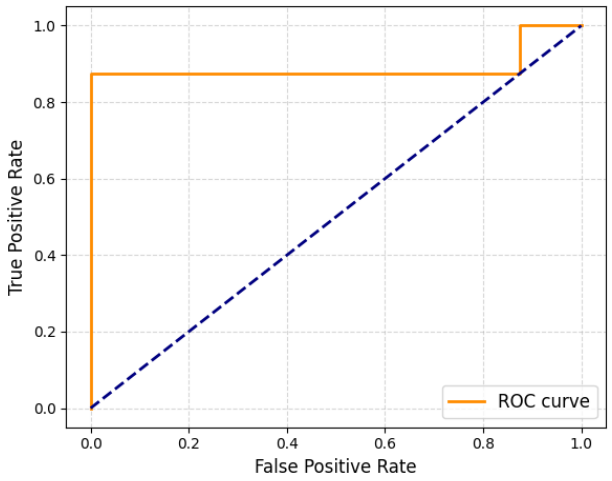

Figure 12 – ROC Curve for the SVM classifier based on feature pair e_{12}&$\tilde{e}_{10}$

A source: Calculated by the authors.

– Based on linear transient characteristics:

$$\left(e_{16} = \max_{m\in[0,M]} |\hat{h}_1(t_m)|\right) \& \left(\tilde{e}_{16} = \max_{m\in[0,M]} |\hat{g}_1(t_m)|\right); \quad (15)$$

– Based on quadratic transient characteristics:

$$\left(e_{12} = \min_{m\in[0,M]} \hat{h}_2'(t_m, t_m)\right) \& \left(\tilde{e}_{12} = \min_{m\in[0,M]} \hat{g}_2'(t_m, t_m)\right); \quad (16)$$

– Based on a combination of linear and quadratic transient characteristics:

$$\left(e_2 = \sum_{m=0}^{M} |\hat{h}_2(t_m, t_m)|\right) \& \left(\tilde{e}_5 = \arg\max_{m\in[0,M]} \hat{g}_1'(t_m)\right); \quad (17)$$

$$\left(e_6 = \max_{m\in[0,M]} \hat{h}_2'(t_m, t_m)\right) \& \left(\tilde{e}_4 = \max_{m\in[0,M]} \hat{g}_1'(t_m)\right); \quad (18)$$

$$\left(e_{10} = \min_{m\in[0,M]} \hat{h}_1'(t_m)\right) \& \left(e_{12} = \min_{m\in[0,M]} \hat{h}_2'(t_m, t_m)\right). \quad (19)$$

Feature space W and $\tilde{W}$: In the feature spaces W and $\tilde{W}$ combining horizontal and vertical data, a maximum PCR of 87.5% was observed for the feature pair w_1&$\tilde{w}_3$.

3.7 Cross-Validation of the SVM Classifier

To evaluate the generalization capability and robustness of the developed SVM

classifiers, a 32-fold Stratified cross-validation procedure was applied. This approach ensured a balanced representation of both psychophysiological states ("Morning" and "Evening") in each training and testing subset, preserving the proportional distribution of samples across folds.

The initial dataset included eight experimental series for each state and for each experimental orientation (Model1 and Model2). To expand the sample and prevent overfitting, additive Gaussian noise of 1%, 3%, and 5% was introduced into the data. This augmentation significantly increased the dataset volume and allowed for a more reliable estimation of the classifier's performance under noisy conditions.

3.7.1 Dataset Based on Model1

Feature space E_0: the maximum PCR = 85.94% was obtained for the feature pair

$$\left(e_{10} = \min_{m\in[0,M]} \hat{h}_1'(t_m)\right) \& \left(e_{12} = \min_{m\in[0,M]} \hat{h}_2'(t_m, t_m)\right); \quad (20)$$

indicating moderate class separability between the "Morning" and "Evening" states. The corresponding confusion matrix and ROC curve are shown in Fig. 13 and Fig. 14, respectively.

Feature space W: the highest recognition accuracy was achieved for the feature pair w_4&w_8, with PCR = 87.5%.

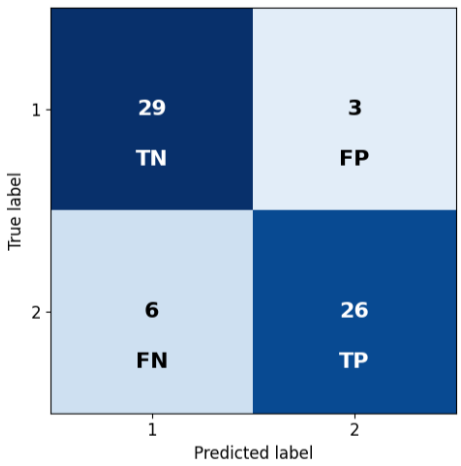

Figure 13 – Confusion Matrix for the classifier based on feature pair e_{10}&e_{12}

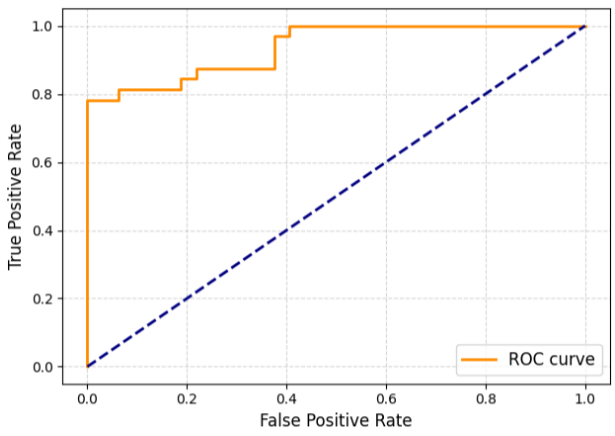

Figure 14 – ROC Curve for the SVM classifier based on feature pair e_{10}&e_{12}

A source: Calculated by the authors.

3.7.2 Dataset Based on Model2

Feature space $\tilde{E}_0$: the highest probability of correct recognition (PCR = 93.75%) was achieved for the feature pair:

$$\left(\tilde{e}_{13} = \arg\min_{m\in[0,M]} \hat{g}_2^{'}(t_m, t_m)\right) \& \left(\tilde{e}_{18} = \max_{m\in[0,M]} |\, \hat{g}_2(t_m, t_m)\,|\right); \quad (21)$$

Comparable performance values (PCR = 87.5%) were observed for the pairs:

$$\left(\tilde{e}_2 = \sum_{m=0}^{M} |\, \hat{g}_2(t_m, t_m)\,|\right) \& \left(\tilde{e}_{11} = \arg\min_{m\in[0,M]} \hat{g}_1^{'}(t_m)\right); \quad (22)$$

$$\left(\tilde{e}_5 = \arg\max_{m\in[0,M]} \hat{g}_1^{'}(t_m)\right) \& \left(\tilde{e}_{13} = \arg\min_{m\in[0,M]} \hat{g}_2^{'}(t_m, t_m)\right). \quad (23)$$

Compared with Section 6.2 (PCR = 87.5%), the PCR increased by 6.25%. The corresponding confusion matrix and ROC curve are presented in Fig. 15 and Fig. 16, respectively.

Feature space $\tilde{W}$: the maximum PCR of 90.62% was obtained for the feature pair $\tilde{w}_1\&\tilde{w}_3$. A slightly lower value of 89.06% was observed for the pair $\tilde{w}_7\&\tilde{w}_9$. Compared with Section 6.2 (PCR = 93.75%), the classification accuracy decreased.

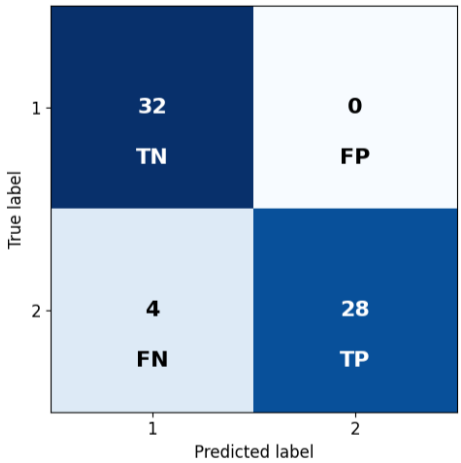

Figure 15 – Confusion Matrix for the classifier based on feature pair $\tilde{e}_{13}\&\tilde{e}_{18}$

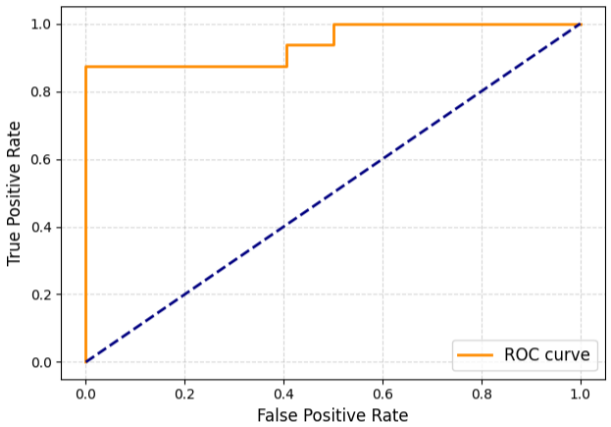

Figure 16 – ROC Curve for the SVM classifier based on feature pair $\tilde{e}_{13}\&\tilde{e}_{18}$

A source: Calculated by the authors.

3.7.3 Dataset Based on Model1 and Model2

Feature space E_0 and $\tilde{E}_0$: the highest PCR approached 100% for the feature pair:

$$\left(e_{12} = \min_{m\in[0,M]} \hat{h}_2^{'}(t_m, t_m)\right) \& \left(\tilde{e}_{10} = \min_{m\in[0,M]} \hat{g}_1^{'}(t_m)\right); \quad (24)$$

Additional feature pairs yielded PCR values:

PCR = 98.44% :

$$\left(e_{12} = \min_{m\in[0,M]} \hat{h}_2^{'}(t_m, t_m)\right) \& \left(\tilde{e}_{12} = \min_{m\in[0,M]} \hat{g}_2^{'}(t_m, t_m)\right); \quad (25)$$

PCR = 92.19% :

$$\left(e_4 = \max_{m\in[0,M]} \hat{h}_1^{'}(t_m)\right) \& \left(\tilde{e}_4 = \max_{m\in[0,M]} \hat{g}_1^{'}(t_m)\right); \quad (26)$$

$$\left(e_{16} = \max_{m\in[0,M]} |\hat{h}_1(t_m)|\right) \& \left(\tilde{e}_{18} = \max_{m\in[0,M]} |\hat{g}_2(t_m, t_m)|\right). \quad (27)$$

Feature space W and $\tilde{W}$: the highest PCR of 90.62% was achieved for the feature pairs $w_2 \& \tilde{w}_5$.

The corresponding confusion matrix and ROC curve are illustrated in Fig. 17 and Fig. 18, confirming the stability of classification performance across the combined feature spaces and consistency with non-validated trends.

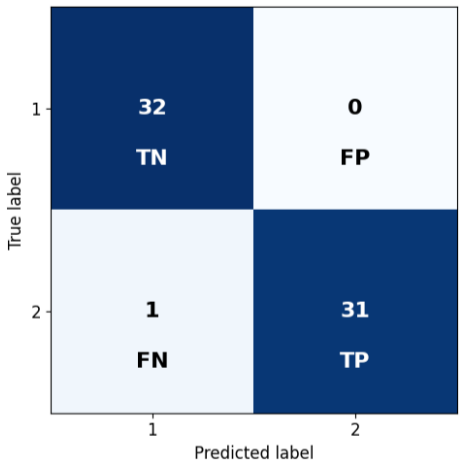

Figure 17 – Confusion Matrix for the classifier based on feature pair $e_{12} \& \tilde{e}_{12}$

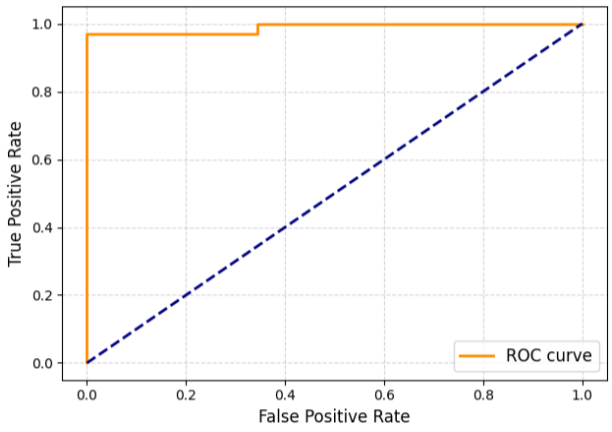

Figure 18 – ROC Curve for the SVM classifier based on feature pair $e_{12} \& \tilde{e}_{12}$

A source: Calculated by the authors.

All maximum PCR values for SVM classification, both before and after applying 32-fold cross-validation, are summarized in Table 3.

Table 3 – Summary of maximum PCR values for SVM classifiers with and without 32-fold cross-validation

Dataset	E_0 and $\tilde{E}_0$	W and $\tilde{W}$	E_0 and $\tilde{E}_0$ (32-fold CV)	W and $\tilde{W}$ (32-fold CV)
Model1	87.5%	87.5%	85.94%	87.5%
Model2	87.5%	93.75%	93.75%	90.62%
Model1 & Model2	93.75%	87.5%	~100%; 98.44%	90.62%

A source: Calculated by the authors.

Summary and conclusions.

The present research examined the human eye movement system (EMS) through nonlinear integral models expressed as quadratic Volterra polynomials in the form of multidimensional transient characteristics. Experimental "input-output" data, collected using advanced eye-tracking technology, enabled the identification of EMS models with three step test signals of varying amplitudes.

The EMS models were constructed on the basis of experimental datasets obtained for two orientations: horizontal (Model1) and vertical (Model2). Correspondingly, two categories of diagnostic feature spaces were formed: heuristic (E_0 – Model1 and $\tilde{E}_0$ – Model2) and wavelet-based (W – Model1 and $\tilde{W}$ – Model2). To evaluate the psychophysiological state of a person, statistical machine learning approaches were applied within these constructed feature spaces. Training datasets were prepared separately for E_0 and $\tilde{E}_0$, as well as for W and $\tilde{W}$, along with a combined dataset integrating both experimental orientations. Comprehensive computer modeling of feature combinations was carried out, which made it possible to identify diagnostically informative feature pairs with maximum probability of correct recognition (PCR).

The novelty of this study is associated with the experimental design: classification analysis was performed not only on horizontal EMS data but also extended to vertical experiments and the integrated dataset. This extension made it possible to reveal how the orientation of the experiment affects classification performance.

The obtained results show that the support vector machine (SVM) classifiers

demonstrated stable recognition capability across all feature spaces. For the separate experimental datasets, the maximum probability of correct recognition (PCR) reached 87.5% for Model1 in both E_0 and W spaces, and 93.75% for Model2 in the $\tilde{W}$ space. When the horizontal and vertical datasets were combined, the recognition accuracy increased, achieving a maximum PCR of 93.75% in the heuristic feature space. This confirms that combining experimental data obtained in different orientations enhances the diagnostic informativeness of the features and improves class separability between the “Morning” and “Evening” states.

The application of 32-fold cross-validation further verified the reliability and generalization capability of the SVM classifiers. The datasets were augmented with samples containing additive Gaussian noise (1%, 3%, and 5%), allowing an assessment of model robustness under realistic variability. For the combined dataset, the highest PCR of 98.44% was achieved in the feature space E_0 and $\tilde{E}_0$, whereas in the space W and $\tilde{W}$, the maximum PCR reached 90.62%. These results confirm that incorporating cross-validation and noise-augmented data provides a more objective evaluation of classifier performance and enhances the reliability of recognition outcomes.

In conclusion, this study demonstrates the influence of experimental orientation on recognition outcomes and confirms the diagnostic significance of the constructed feature spaces. The results create a solid basis for further refinement of machine learning techniques for psychophysiological state evaluation, including the use of integrated horizontal and vertical datasets to enhance classifier stability and generalization ability.